Acta Crystallographica Section D
Biological Crystallography
ISSN 0907-4449

Mapping the conformational space accessible to BACE2 using surface mutants and cocrystals with Fab fragments, Fynomers and Xaperones

David W. Banner,[a]‡§ Bernard Gsell,[a]‡ Jörg Benz,[a] Julian Bertschinger,[b] Dominique Burger,[a] Simon Brack,[b] Simon Cuppuleri,[a]§ Maja Debulpaep,[c,d] Alain Gast,[a] Dragan Grabulovski,[b] Michael Hennig,[a] Hans Hilpert,[a] Walter Huber,[a] Andreas Kuglstatter,[a] Eric Kusznir,[a] Toon Laeremans,[c,d] Hugues Matile,[a] Christian Miscenic,[a] Arne C. Rufer,[a] Daniel Schlatter,[a] Jan Steyaert,[c,d] Martine Stihle,[a] Ralf Thoma,[a] Martin Weber[a] and Armin Ruf[a]*

[a]pRED Pharma Research and Early Development, Small Molecule Research, Discovery Technologies, F. Hoffmann-La Roche Ltd, 4070 Basel, Switzerland, [b]Covagen AG, Wagistrassse 25, 8952 Zurich-Schlieren, Switzerland, [c]Structural Biology Brussels, Vrije Universiteit Brussel, Pleinlaan 2, 1050 Brussels, Belgium, and [d]Structural Biology Research Centre, VIB, Pleinlaan 2, 1050 Brussels, Belgium

‡ These authors contributed equally.
§ These Roche contributors now have other affiliations.

Correspondence e-mail: armin.ruf@roche.com

Received 25 January 2013
Accepted 7 March 2013

PDB References: BACE2, surface mutant, apo, 3zkg; inhibited, 3zki; Fab complex, uninhibited, 3zkm; inhibited, 3zkn; Xaperone XA4813 complex, uninhibited, 3zkq; inhibited, 3zks; ternary Xaperone complex, 3zkx; Fynomer complex, 3zl7; BACE1 with ligand, 3zov

The aspartic protease BACE2 is responsible for the shedding of the transmembrane protein Tmem27 from the surface of pancreatic β-cells, which leads to inactivation of the β-cell proliferating activity of Tmem27. This role of BACE2 in the control of β-cell maintenance suggests BACE2 as a drug target for diabetes. Inhibition of BACE2 has recently been shown to lead to improved control of glucose homeostasis and to increased insulin levels in insulin-resistant mice. BACE2 has 52% sequence identity to the well studied Alzheimer's disease target enzyme β-secretase (BACE1). High-resolution BACE2 structures would contribute significantly to the investigation of this enzyme as either a drug target or anti-target. Surface mutagenesis, BACE2-binding antibody Fab fragments, single-domain camelid antibody V_HH fragments (Xaperones) and Fyn-kinase-derived SH3 domains (Fynomers) were used as crystallization helpers to obtain the first high-resolution structures of BACE2. Eight crystal structures in six different packing environments define an ensemble of low-energy conformations available to the enzyme. Here, the different strategies used for raising and selecting BACE2 binders for cocrystallization are described and the crystallization success, crystal quality and the time and resources needed to obtain suitable crystals are compared.

1. Introduction

BACE2 is a membrane-bound aspartic protease that was so named because of its 52% sequence identity to the important Alzheimer's disease drug target β-site amyloid precursor protein cleaving enzyme 1 (BACE1 or β-secretase). The exact physiological functions of BACE2 remain to be elucidated. Recently, it has been shown that BACE2 cleaves off the ectodomain of the pro-proliferative plasma-membrane protein Tmem27 on pancreatic β-cells (Esterházy *et al.*, 2011), leading to two cleavage products: a 25 kDa N-terminal 'shed fragment' that is released into the extracellular space and a 22 kDa C-terminal fragment that remains in the membrane and that is rapidly degraded (Akpinar *et al.*, 2005). Overexpression of Tmem27 has been reported to increase β-cell proliferation *in vitro* and pancreatic β-cell mass *in vivo* (Akpinar *et al.*, 2005), and to augment glucose-stimulated insulin secretion (Fukui *et al.*, 2005). Because the shedding process inactivates the β-cell proliferating activity of Tmem27, a role for BACE2 in the control of β-cell maintenance was immediately suggested. This has since been confirmed: mice with functionally inactive BACE2 and insulin-resistant mice treated with a BACE2 inhibitor both display improved β-cell mass and improved control of glucose homeostasis due to increased insulin levels (Esterházy *et al.*, 2011). BACE2 may therefore be of high importance in drug discovery as a target for the expansion of

functional pancreatic β-cell mass in diabetes. Abdul-Hay *et al.* (2012) reported that BACE2 degrades the amyloid-producing Aβ peptides and thus may turn out to be an important anti-target for selective inhibitors of BACE1 in Alzheimer's disease. While numerous high-resolution crystal structures have been reported for BACE1 (Hong *et al.*, 2000; Patel *et al.*, 2004), high-resolution structures of BACE2 have not been published. To date, the structure of BACE2 is only known in complex with a ligand that clearly promotes the formation of a highly symmetric tetramer *via* a hydrophobic interaction with Leu327 of the next molecule related by a local dyad (Ostermann *et al.*, 2006). Consequently, this crystal form cannot be used for ligand-binding studies and further provides only one example of the enzyme conformation. The resolution of this structure is only 3.1 Å, even though an artificial maturation site was introduced to obtain more homogenous mature protease for crystallization. As BACE1 displays many different conformations of the 'flap' over the active site and of other loops forming the active site (Patel *et al.*, 2004; Xu *et al.*, 2012), BACE2 might be expected to show similar conformational variability.

Iterative cocrystal structures of target proteins in complex with ligands form the basis for rational drug design, which achieves its highest efficiency if the structures are obtained quickly and at high resolution. However, obtaining cocrystal structures is often difficult or impossible for certain ligands, even when crystallization of the protein has already been well established (Danley, 2006). Robust crystallization systems are thus required that reproducibly and rapidly yield well diffracting crystals of all desired protein–ligand complexes. Despite best efforts, instances are known in the pharmaceutical industry where crystallographers are forced to go back to the costly and time-consuming process of co-expression, co-purification and cocrystallization for each new ligand for some target proteins, as the protein variant or the crystals available prevent faster ways of obtaining the desired structure (Hassell *et al.*, 2007). If the bound ligands influence the conformation of the target protein, cocrystallization of the ligands with the protein is preferred over soaking ligands into apo crystals, where packing interactions might prevent the protein from adopting the conformation in which the ligand binds or where the ligands might induce changes in protein conformation that destroy the crystals. On the other hand, crystallization space is often narrow and not compatible with the high ligand and solvent concentrations required to achieve good ligand occupancy. It is not uncommon that cocrystal structures cannot be obtained for certain compounds for a given crystal form, whereas other compounds, for example from different structural classes, easily yield structures of complexes (Danley, 2006). The structures of problematic ligands may often be obtained from crystals with a different packing, from crystals grown at a different pH where ligand solubility is higher or where subtle differences in conformation, accessibility or mobility of the inhibitor-binding pocket in the crystals allow binding without destroying the crystal. In addition to the deletion of mobile protein regions, several specific techniques have been used to alter or enlarge the protein surfaces available for crystal lattice contacts in order to improve crystals or change the packing. Mittl *et al.* (1994) improved a lattice contact in glutathione reductase crystals by introducing an intermolecular salt bridge, resulting in facilitated nucleation but not in improved diffraction. Mutation of a surface serine to cysteine in 6-phospho-β-galactosidase enabled the determination of both the apo structure (*via* a heavy-atom derivative) and a 'substrate-bound' conformation (from a disulfide-bridged dimer; Wiesmann *et al.*, 1995). Exchange of a surface lysine to a bulky hydrophobic isoleucine led to well diffracting crystals of a cyclophilin (Schlatter *et al.*, 2005). A more general approach is the introduction of 'surface-entropy mutations'; this has now established itself and is widely and routinely used to improve protein crystallization (Derewenda, 2004). More recently, cocrystallization with protein binders as crystallization helpers has received much attention. This approach is widely applicable, although it may be more labour-intensive than that of point mutation of surface residues.

The potential of antibody Fab fragments (Fabs) to increase the rigid protein surface available for crystal lattice interaction was realised almost 20 years ago (Kovari *et al.*, 1995), and the Michel group has pioneered their use in the crystallization of transmembrane proteins (Hunte & Michel, 2002). Fabs have frequently been applied as crystallization helpers. Fabs for use in crystallization can be derived from mouse monoclonal antibodies or by selection from immunoglobulin gene libraries by techniques such as phage display or ribosome display. The antigen-binding fragments of camelid heavy-chain-only antibodies are smaller (only one Ig domain; 12–15 kDa) and more rigid than the Fab fragments from normal antibodies and are known as V_HHs, or Nanobodies or Xaperones when used for crystallization (Hamers-Casterman *et al.*, 1993; Tereshko *et al.*, 2008). Xaperones have successfully been applied to crystallize difficult proteins such as unstructured domains, transmembrane proteins and protein complexes (Loris *et al.*, 2003; Spinelli *et al.*, 2006; Tereshko *et al.*, 2008; Lam *et al.*, 2009; Korotkov *et al.*, 2009; Rasmussen, Choi *et al.*, 2011; Domanska *et al.*, 2011; Baranova *et al.*, 2012), culminating in the structure of the active β2AR receptor in complex with heterotrimeric G proteins (Rasmussen, DeVree *et al.*, 2011; Steyaert & Kobilka, 2011). Xaperones may be raised by immunizing llamas, and the single-domain Xaperone cDNA can easily be amplified from blood samples, inserted into phage-display libraries, expressed in *Escherichia coli* and characterized using standard techniques (Muyldermans, 2001). Src-homology domains 3 (SH3 domains) are found in many proteins and mediate protein–protein interaction in signal transduction pathways. The human Fyn kinase SH3 domain is a small five-stranded β-barrel (63 amino acids) that is highly stable, lacks cysteine residues and presents the Src and RT loops that are responsible for protein–protein interaction (Grabulovski *et al.*, 2007). Fyn SH3 domains selected by phage display from libraries with randomized interaction-loop sequences are called Fynomers and can be produced in *E. coli*. Recently, the isolation of Fynomers binding to the serine protease chymase has been reported and the first Fynomer–chymase cocrystal structures have been published (Schlatter *et al.*, 2012). Other

classes of binding proteins have also been reported as crystallization helpers. DARPins are based on ankyrin-repeat modules (Sennhauser & Grütter, 2008), monobodies are derived from the tenth fibronectin type III domain of human fibronectin (Koide *et al.*, 2007), Affibodies are derived from the immunoglobulin-binding protein A (Nygren, 2008) and anticalins are derived from lipocalins (Gebauer & Skerra, 2012). The application of DARPins, Affibodies and anticalins in crystallization has been reviewed by Gilbreth & Koide (2012) and the use of Xaperones for crystallization has been reviewed by Steyaert & Kobilka (2011). In this study, we generated antibody Fab fragments, Xaperones and Fynomers in order to obtain BACE2 crystals that yield high-resolution structures.

The present study had several objectives. The first was to obtain the first high-resolution structure of BACE2 to support structure-based inhibitor design as either a drug target or anti-target. The second was to obtain several independent structures of BACE2 in order to map different conformational states of the enzyme, since from the biochemical properties of BACE2 its intrinsic flexibility has been suggested to possibly be higher than those of other flexible aspartic proteases (Ostermann *et al.*, 2006). The third was to create a tool chest of BACE2 crystals grown from solutions with different pH and with different packing interactions and different active-site conformations that could yield high-resolution structures. This might serve to repeatedly and rapidly obtain cocrystal structures with previously intractable inhibitor series. Further, multiple re-determination of inhibitor-complex structures in different crystal-packing environments was expected to give more confidence in the physiological relevance of observed inhibitor conformations. Finally, we wanted to evaluate and compare different protein-crystallization technologies side by side and to derive criteria for the selection of the most suitable crystallization strategy for a given protein. We report eight structures here and also report how the different cocrystallization helpers differed with regard to the properties, crystallization success, crystal quality and time and resources needed to obtain suitable crystals.

2. Methods

2.1. BACE2 mutagenesis, expression and purification

Human BACE2 (residues 20p–398) with the secretion signal missing and with an artificial factor Xa cleavage site for maturation was cloned, expressed and purified for crystallization as described by Ostermann *et al.* (2006). (Here, we use the same numbering scheme, which is 62 residues less than that of full-length pro-BACE2; UniProt Q95YZ0.) All BACE2 constructs lacked the secretion signal and were expressed in *E. coli* BL21 (DE3) cells at 310 K as inclusion bodies. Isolated and purified inclusion bodies were dissolved in 50 m*M* Tris–HCl pH 8.0 containing 8 *M* guanidine–HCl and 30 m*M* DTT. Protein concentrations were measured by RP-HPLC (Poroshell 300SB-C8; 1 × 75 mm) and were adjusted to a final concentration of 2 mg ml^{-1}. Refolding was performed using a two-step dilution protocol. 50 ml inclusion-body solution was diluted 20-fold in 3 *M* guanidine–HCl, 0.7 *M* arginine, 1 m*M* glutathione (reduced), 0.5 m*M* glutathione (oxidized) adjusted with NaOH to pH 10.4 at 277 K. After overnight incubation, a second 20-fold dilution at room temperature in 1 *M* NaCl, 0.7 *M* arginine, 1 m*M* glutathione (reduced), 0.5 m*M* glutathione (oxidized) adjusted with NaOH to pH 9.4 was made. The refolding solution was incubated for 3 d at room temperature and was then concentrated 20-fold using TFF cross-flow filtration (10 kDa). The solution was adapted to 1.5 *M* ammonium sulfate and centrifuged at 20 000*g* for 30 min. The clear supernatant was loaded onto a Toyopearl Butyl 650M (2.6 × 5 cm) column equilibrated in 10 m*M* Tris–HCl pH 8.0, 1 *M* NaCl, 1.5 *M* ammonium sulfate. Elution was performed with a decreasing ammonium sulfate concentration and the BACE2-containing fractions were pooled and adjusted to pH 8.3. In order to activate the protein, factor Xa was added at a molar ratio of 1:100 and the protein pool was dialyzed for 4 d at 277 K against 10 m*M* Tris–HCl pH 8.0, 150 m*M* NaCl. Activated BACE2 was concentrated and loaded onto a Superdex 200 GL 10/300 column equilibrated in 25 m*M* bis-tris propane pH 7.0, 150 m*M* NaCl, 10% glycerol, 0.35% CHAPS. Pooled protein fractions were chromatographed using a Fast Desalting HR 10/10 column in order to exchange the buffer to 20 m*M* sodium acetate pH 4.1, 10% glycerol, 0.35% CHAPS and to be compatible with a subsequent cation-exchange chromatography using Fractogel EMD SO3-650 (1 × 4 cm). Elution was performed with a linear gradient from 0 to 1 *M* NaCl in 20 column volumes. BACE2-containing fractions were pooled and the pH was adjusted to 7.0 with 3 *M* Tris. BACE2 was finally polished using size-exclusion chromatography (SEC) on a TSK G3000SW (21.4 × 600 mm) column equilibrated in 20 m*M* HEPES–NaOH pH 7.0, 150 m*M* NaCl. The protein purity was 99% according to RP-HPLC and the final yield was about 15 mg purified active protease from 1 g of inclusion bodies.

We used a mutational surface-engineering approach to enhance the BACE2 crystal quality. However, in contrast to classical surface-entropy reduction (Derewenda, 2004) and instead of using the *SERp* server, which looks for clusters of charged residues in protein sequences (Goldschmidt *et al.*, 2007), we started from the available crystal structure of BACE2 and also considered surface-residue mutations that had led to improved crystals of the homologue BACE1 (Kuglstatter *et al.*, 2008). 11 single mutants were designed that replaced flexible lysine and glutamic acid residues on the BACE2 surface distant from the substrate-binding pocket by alanines: E71A, E120A, E122A, K198A, K218A, E259A, E269A, K295A, E287A, K362A and E389A. These include lysine and glutamic acid residues adjacent in space on the BACE2 surface that are not clustered in sequence. Also, mutants that would destroy a dimer-forming contact from Glu120 and Glu122 to Lys295 and Arg310 present in the previously published BACE2 crystals were judged to help in discovering better crystal forms. Further, two double mutants E71A/R77A and K207R/K362A and the triple mutant E120A/E122A/K295A that removed charged clusters on the surface

were proposed. Retrospective analysis has shown that we touched on all three clusters (K207A/E208A/E209A, Q361A/K362A and E287A) that are proposed from the sequence alone by the *SERp* server, but we note that our structure-based surface-mutagenesis approach also suggested additional surface regions, and in fact the E269A mutant which gave the best crystals (see below) was not proposed by the *SERp* server (Goldschmidt *et al.*, 2007).

2.2. Production of the protein binders

The anti-BACE2 monoclonal antibodies (MABs) were obtained by immunization of Swiss albino mice at 2–3 week intervals with human BACE2 244–333 (TTLL . . . ECYR; Abnova; NP-036237) attached to a GST tag. Animals with serum that was more reactive for the immunogen than for GST alone were selected and MABs were prepared as described in Hausammann *et al.* (2013). MABs were digested with papain at 293 K for 1 d, the reaction was stopped using the cysteine protease inhibitor E64 and the Fab was separated from Fc and undigested MAB by sequential chromatography on a protein A column with a final SEC polishing step. The BACE2–Fab complexes were formed by mixing BACE2 and Fab in a molar ratio of 1:1.5. The complexes were purified by SEC (TSK G3000SW) and the complex-containing fractions were selected by simultaneous multi-angle light-scattering analysis (MALS; TriStar, Wyatt).

Antibody MAB 1/9 was sequenced under contract by GenScript (http://www.genscript.com). Total RNA was extracted from frozen hybridoma cells and antibody cDNA was generated by RT-PCR and sequenced using standard technology.

BACE2-specific Fynomers were obtained using the procedure described by Grabulovski *et al.* (2007). In summary, starting from a phage library with two randomized loops (RT and Src) and different loop lengths, three rounds of panning and phage amplification were performed using streptavidin-immobilized biotinylated BACE2. Phage clones were screened by phage ELISA and their loop sequences were analyzed. Clones were selected and used as templates for one round of affinity maturation with specifically designed sub-libraries. The Fynomer sequences were cloned into bacterial expression vector (pQE12) with a C-terminal 6×His tag. The Fynomers were expressed, small-scale purified and screened by ELISA and Biacore. For crystallization, selected Fynomers were expressed in *E. coli* and isolated from the lysate on a Talon column with subsequent size-exclusion chromatography on Superdex 75 (Schlatter *et al.*, 2012). The buffer was exchanged to PBS and the purified Fynomers were stored in aliquots at 253 K or on ice for immediate use.

BACE2-specific Xaperones were generated by a protocol similar to that described by Domanska *et al.* (2011). In brief, one llama was immunized four times with active human BACE2 13–398 and another llama was immunized with the same BACE2 inhibited by the commercially available non-specific BACE inhibitor (CAS 797035-11-1). 4 and 8 d after the final antigen boost, peripheral blood lymphocytes were extracted and their mRNA was purified and converted into cDNA *via* RT-PCR. The Xaperone repertoire was cloned into a phage-display/expression vector (pMESy4) containing a C-terminal 6×His and EPEA tag, resulting in two Xaperone libraries. Xaperones that bind to BACE2 were identified in multiple biopanning experiments. In subsequent selection rounds the target was presented either immobilized directly on a solid phase, immobilized *via* antibody or immobilized *via* neutravidin capturing. Xaperones that did not retain BACE2 binding in the presence of the inhibitor were discarded. For characterization, the His-tagged Xaperones were expressed periplasmically in *E. coli* WK6 cultures on a 24-well plate and purified by Ni–NTA Superflow. The stoichiometry of binding was assessed by mixing BACE2 with a 1.5-fold excess of each of six Xaperones, incubating for 1 h at room temperature, separating the complex from the free Xaperone by size-exclusion chromatography and determining the stoichiometry of the complexes by RP-HPLC. For subsequent large-scale preparation, selected Xaperones were first purified directly from the periplasmic extract on a HisTrap column and chromatographed by size-exclusion chromatography.

2.3. SPR and AUC measurements

Surface plasmon resonance (SPR) binding measurements were performed using Biacore 3000 instruments. 400–700 response units (RU) of BACE2 were immobilized on CM5 sensor chips by amine coupling. The immobilization buffer was sodium acetate pH 4.6 at 298 K and activation of the surface was with NHS/EDC for 7 min. All binding experiments were performed at 298 K; 10 m*M* HEPES, 150 m*M* NaCl, 3 m*M* EDTA, 0.01% P20 pH 7.4–7.6 was used as the running buffer.

For determination of kinetic and binding constants, a series of five different concentrations of protein binder (Fynomer, Xaperone or Fab) was prepared and binder association and dissociation were measured in alternating cycles with contact times of 2.5 min for association. Kinetic and thermodynamic parameters were obtained by fitting the sensograms to an appropriate model in the *BIAevaluation* software.

For the competition experiment between two Xaperones the saturation response was determined for each of them individually by injecting solutions at a concentration of ten times the K_d. Subsequently, the response of a mixture of the two Xaperones was determined. The injected mixture contained each Xaperone at a concentration of ten times its K_d. Competition was assessed by comparison of the individual responses of the Xaperones with the response of their mixture (Perspicace *et al.*, 2009). A response of the mixture equal to the sum of the individual responses indicates no competition, *i.e.* separated binding sites. A response of the mixture approximating to an individual response is indicative of competition, *i.e.* the binding sites are identical or at least overlap significantly (see also Supplementary Fig. S1[1]).

[1] Supplementary material has been deposited in the IUCr electronic archive (Reference: TZ5028). Services for accessing this material are described at the back of the journal.

Table 1
Data-collection and refinement statistics.

Each data sets was collected from one single crystal. Values in parentheses are for the highest resolution shell.

Crystallization aid	E269A	E269A	Fab 1/9	Fab 1/9	XA4813	XA4813	XA4813 + XA4815	Fynomer 2B-H11
Ligand	RO5464694	Bis-tris propane	RO5464694	—	RO5464694	Bis-tris propane	—	Fynomer
PDB code	3zki	3zkg	3zkn	3zkm	3zks	3zkq	3zkx	3zl7
Data collection								
Space group	$P2_1$	$P2_1$	$P2_1$	$P2_12_12_1$	$P2_12_12_1$	$P2_12_12_1$	$I222$	$P4_32_12$
Unit-cell parameters								
a (Å)	47.3	46.9	81.9	67.9	64.1	64.1	63.4	84.8
b (Å)	89.2	88.5	68.1	161.1	74.8	74.8	153.8	84.8
c (Å)	98.9	98.6	160.9	163.2	108.7	109.2	247.2	128.1
$\alpha = \gamma$ (°)	90	90	90	90	90	90	90	90
β (°)	97.0	96.5	92.5	90	90	90	90	90
Resolution (Å)	49.1–2.40 (2.50–2.40)	32.8–1.90 (1.99–1.90)	45.7–2.00 (2.05–2.00)	44.9–1.80 (1.89–1.80)	44.4–2.11 (2.21–2.11)	44.5–1.51 (1.61–1.51)	34.7–2.37 (2.50–2.37)	43.77–3.01 (2.91–3.01)
No. of unique reflections	31592 (3685)	61792 (8067)	117848 (15068)	139962 (11607)	28977 (3949)	83053 (14315)	49549 (7117)	10238 (1012)
Completeness (%)	98.6 (99.7)	98.1 (99.7)	98.3 (93.5)	84.3 (52.7)	94.0 (100)	99.8 (99.6)	99.9 (99.8)	94.5 (100)
Multiplicity	2.54 (2.53)	2.57 (2.61)	3.7 (3.3)	2.9 (1.4)	6.1 (6.4)	6.6 (6.4)	6.6 (6.7)	11.6 (12.7)
R_{merge} (%)	8.2 (44.3)	12.9 (35.2)	7.7 (56.4)	7.0 (41.0)	16.7 (75.8)	7.1 (69.7)	8.6 (88.5)	13.2 (73.8)
$\langle I/\sigma(I)\rangle$	10.4 (2.2)	5.1 (2.5)	10.5 (2.0)	9.8 (1.9)	8.2 (1.26)	10.9 (1.4)	13.4 (1.2)	12.9 (1.9)
Wilson B (Å^2)	40.0	29.8	34.1	28.0	34.7	27.7	62.2	73.4
Refinement								
Resolution (Å)	49.1–2.40 (2.46–2.40)	32.8–1.90 (1.95–1.90)	45.7–2.00 (2.05–2.00)	44.86–1.85 (1.90–1.85)	44.42–2.11 (2.16–2.11)	44.47–1.51 (1.55–1.51)	34.70–2.37 (2.43–2.37)	43.77–3.20 (3.58–3.20)
No. of reflections	29125 (2186)	58113 (4443)	108982 (7340)	123528 (6024)	25928 (1960)	75161 (5316)	49387 (3565)	7602 (1954)
R_{cryst}/R_{free} (%)	18.6/24.1 (29.8/42.6)	23.1/27.3 (29.2/35.7)	20.6/25.1 (36.7/45.7)	21.2/24.5 (31.9/38.2)	21.1/26.0 (31.7/33.1)	19.1/22.3 (36.2/37.5)	18.5/20.9 (26.8/27.2)	28.0/30.6 (40.3/35.0)
No. of non-H atoms								
Protein	5656	5633	12520	12647	3670	3814	4541	3334
Ligand/ion	62	19	31/50	30	31	19/1	5	—
Water	248	302	842	953	150	419	312	22
Mean temperature factors (Å^2)								
Protein	35.7	27.5	29.5	21.9	33.3	31.0	66.7	80.2
Ligand/ion	31.6	39.2	43.3/55.5	41.1	35.2	39.4/23.9	72.9	—
Water	31.3	28.6	34.2	29.8	31.7	36.4	70.4	57.4
R.m.s. deviations								
Bond lengths (Å)	0.009	0.010	0.010	0.011	0.010	0.011	0.010	0.007
Bond angles (°)	1.43	1.38	1.38	1.44	1.45	1.46	1.16	0.94

Analytical ultracentrifugation (AUC) was used in a standard way to confirm the aggregation states of monomers, dimers or trimers (Supplementary Fig. S2).

2.4. BACE2 activity assay

To determine the IC_{50} of the inhibiting Fynomers, a BACE2 FRET assay was performed using a fluorescent substrate (WSEVNLDAEFRC-MR121) in triplicate at room temperature in a final volume of 50 µl in 384-well microtitre plates. All reagents were diluted in the assay buffer: 100 m*M* sodium acetate, 20 m*M* EDTA, 0.05% BSA pH 4.5. The anti-BACE-2 Fynomers were serially diluted and 20 µl of these dilutions was mixed for 10 min with 20 µl human recombinant BACE-2 (final concentration 62.5 n*M*). After addition of 10 µl of the substrate (final concentration 300 n*M*), the plates were shaken for 2 min. The enzymatic reaction was followed in a plate::vision reader (PerkinElmer; excitation wavelength 630 nm; emission wavelength 695 nm) for 30 min in a kinetic measurement detecting an increase of MR121 fluorescence during the reaction time. The slope in the linear range of the kinetics was calculated and the IC_{50} was determined using a four-parameter equation for curve fitting.

2.5. Crystallization and structure determination

The complexes used for cocrystallization were produced by incubating BACE2 with a 1.5 molar excess of the protein-binding molecule for 60 min followed by purification of the complex by size-exclusion chromatography. For crystallization, sitting-drop plates were used in combination with various screens and temperatures. Crystallization droplets contained a 50 or 70% fraction of protein in a total volume of 0.350–2.5 µl. Crystallization batches included heterodimeric complexes of BACE2 with one protein binder and ternary complexes with two different noncompeting binders. Inhibitor complexes were obtained by crystal soaking with 5–25 m*M* inhibitor for between 2 h and 3 d. For data collection, crystals were harvested directly from the screening plates without further optimization. Crystals were harvested with glycerol as a cryoprotectant and were then flash-cooled in liquid nitrogen. Diffraction images were collected at a temperature of 100 K on beamline X10SA (PXII) at the Swiss Light Source (SLS) initially using a MAR225 CCD detector and later using a PILATUS 6M pixel-array detector. Images were processed with *XDS* (Kabsch, 2010) and scaled with *SADABS* (obtained from Bruker AXS) or *SCALA* (Winn *et al.*, 2011). All BACE2 structures were solved by molecular replacement with *Phaser*

(McCoy *et al.*, 2007) initially using the coordinates of human BACE2 (PDB entry 2ewy; Ostermann *et al.*, 2006) as a search model and later the in-house coordinates of highest resolution. Search models were extracted from PDB entries 2aju (cocaine catalytic antibody 7A1 Fab; Zhu *et al.*, 2006), 1fyn (Fyn SH3 domain; Musacchio *et al.*, 1994) or 2xa3 (Nanobody; Hinz *et al.*, 2010). The Fab and Nanobody CDRs and the RT and the Src loops of the Fynomer could easily be traced using *Coot* (Emsley & Cowtan, 2004). The structures were refined with *REFMAC*5 (Murshudov *et al.*, 2011) or *BUSTER* (Smart *et al.*, 2012) and structural modelling was performed with *Coot*, with the *CCP*4 program suite (Winn *et al.*, 2011) being used extensively.

3. Results

3.1. Crystals giving low-resolution data

We were able to obtain crystals belonging to space group *P*321 (unit-cell parameters $a = b = 126$, $c = 121$ Å) using the protein construct described by Ostermann *et al.* (2006) by cocrystallization with the peptidic inhibitor H-4848 (Bachem; Lys-Thr-Glu-Glu-Ile-Ser-Glu-Val-Asn-Sta-Val-Ala-Glu-Phe), but the best resolution obtained was only 3.0 Å. This confirmed the BACE2 structure in PDB entry 2ewy, but the crystals were not suitable for ligand-binding studies. No well diffracting apo structures could be determined. Mutations to improve the contacts in this crystal form ('crystal lattice engineering'; Meher *et al.*, 2009) were considered, but were rejected in favour of the approaches presented below.

3.2. Surface-entropy mutants

Of the 14 BACE2 variants proposed, five were delayed in mutagenesis and three did not express to a high level in inclusion bodies; only the single mutants E269A, E287A and E389A and the double mutant E71A/R77A could be refolded and purified and were subsequently used in crystallization experiments. In the initial screens, the single mutants gave crystals but the double mutant did not. Crystals of the E389A and E287A mutants diffracted to ∼3.5 Å resolution, but the E269A mutant yielded monoclinic crystals which diffracted to better than 2 Å resolution in two instances but generally gave ∼2.4 Å resolution data (Table 1).

There are two independent BACE2 molecules, *A* and *B*, in the asymmetric unit of the BACE2 E269A mutant crystals (see also Supplementary Fig. S3) and these are extremely similar (r.m.s.d. of 0.38 Å for 343 C^{α} pairs as determined using the program *XSAE* with a 1.0 Å cutoff; Broger, 2011). Molecule *A* (Fig. 1) has a bis-tris propane (B3P, not shown) buffer molecule bound in the active site which is not found in molecule *B*, which also has somewhat higher temperature factors. Bis-tris propane was only used in the early stages of protein purification and is only present in residual amounts, but co-purifies with the enzyme. Residues 175–182, 268–269, 284–287 and 324–329 could not be located in electron density for molecule *A* and approximately the same stretches were missing in molecule *B*. Small differences after alignment are observed for residues 108, 183, 227, 264–265, 271–272, 283, 322–323, 330, 341 and 375–376. All these are either in crystal contacts (108, 183 and 227) or adjacent to missing loops, except for 375 and 376, which are in a surface-exposed turn, and 341, which contacts the B3P ligand. Interestingly, the mutated residue Ala269 has no electron density in either molecule, with residues 268–269 absent in molecule *A* and residues 266–269 absent in molecule *B*. Although these residues are close to the local dyad axis, there is no obvious reason why this particular mutant promotes this crystal form. As in PDB entry 2ewy, the loop following residue 174 is missing, but here we also observe higher mobility and missing loops in the C-terminal domain (Fig. 1, Supplementary Fig. S3). Although not particularly tolerant of DMSO, the mutant E269A crystals are suitable for ligand-binding studies, and here we present the complex with RO5464694 (5-(2,2,2-trifluoroethoxy)-pyridine-2-carboxylic acid {3-[(*S*)-2-amino-1,4-dimethyl-6-oxo-1,4,5,6-tetrahydro-pyrimidin-4-yl]-phenyl}-amide; IC_{50} for BACE1, 0.06 μ*M*; IC_{50} for BACE2, 1.2 μ*M*; Table 1).

Consistent with our strategy of initiating several approaches in parallel and selecting the most promising as early as possible, the search for new crystal forms from other mutants was stopped. E269A crystals were used on six occasions to check the binding mode of ligands when other crystal forms had issues with binding mode or occupancy.

3.3. Fab complexes

Four MABs were selected for Fab production, of which three could readily be cleaved to produce Fabs. For each Fab, a 1:1 complex with BACE2 was purified and analyzed by SEC multi-angle light scattering (data not shown). Only one Fab

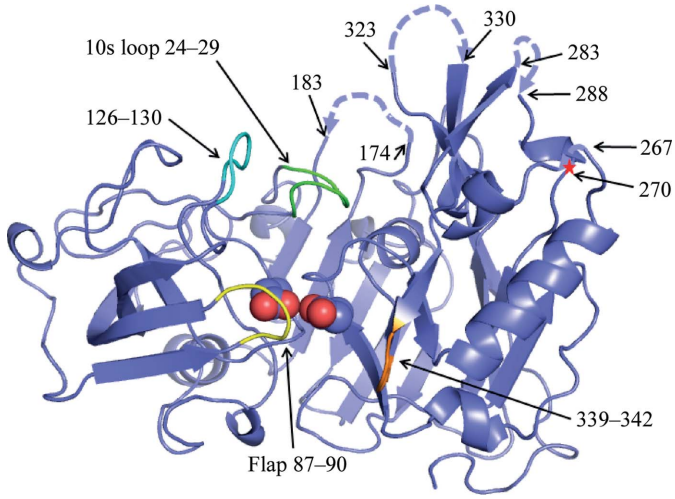

Figure 1
The structure of the E269A mutant of BACE2. One BACE2 monomer is shown coloured slate blue with the catalytic aspartate acids (Asp48 and Asp241) shown as spheres. The 10s loop (Gly24–Gly29) is shown in green, the flap (Tyr87–Gly90) in yellow, loop 126–130 in cyan and loop 339–342 in gold. The N-terminus is at the back. Missing loops are indicated by dotted lines, with the terminal fitted residue numbered; thus, residues 175–182, 268–269, 284–287 and 324–329 could not be located in electron density. A red star indicates the approximate location of the mutated residue Ala269, which had no electron density.

(Fab 1/9) gave BACE2 complex preparations that were monodisperse, and these yielded crystals.

The purified BACE2–Fab 1/9 complex readily gave crystals in various PEG-containing conditions (Supplementary Table S3). The crystals were stacks of plates which were hard to harvest as single crystals. Further optimization of the conditions as well as a search for different crystal forms failed, and the original screening conditions were used to produce over 100 well diffracting crystals. A clear advantage of these Fab 1/9 complex crystals is that they are resistant to soaking in high concentrations (up to 20%) of DMSO, which allows structure determination with inhibitors of low solubility.

Two distinct but closely related crystal forms grew together in the same drop and had similar morphology. Both diffracted to ∼2.0 Å resolution at the SLS and both have been used extensively for ligand-binding studies (Table 1). Both crystal forms contained two molecules per asymmetric unit related by a pseudo-translation. All four molecules are indistinguishable within error (r.m.s.d. of <0.2 Å for all C^{α} atoms except for the flap on refinement without NCS constraints) and only molecule *A* of the apo form (Fig. 2*a*) will be discussed further.

The Fab was raised against residues 244–333 of BACE2 (as the clone was commercially available) and not against the protein prepared for crystallization. The Fab light chain interacts (3.5 Å cutoff) with BACE2 residues 255, 262, 265, 270, 275, 277, 278, 281, 283 and 332, and the heavy chain with residues 268, 269, 270, 272 and 275. The light-chain residues Tyr32-Gly33-His34 (CDR1) displace Phe274 and Trp275 of BACE2 from their location in other BACE2 structures and make hydrophobic interactions with BACE2 residues 332–334 (Fig. 2*b*). Trp275 (which shows two alternative conformations in this particular structure) moves ∼18 Å to interact with both the light and the heavy chains of the Fab (Fig. 2*b*). The nearest Fab residue to the active site is 24 Å from the water bound to the catalytic aspartates. The binding epitope consists of only 14 of the 89 residues used to raise the antibody: presumably, the isolated peptide is able to adopt *in vivo* this local structure in which the disulfide bridge is formed. The contact areas between BACE2 and Fab 1/9 are 819 $Å^2$ for the light chain and 425 $Å^2$ for the heavy chain, giving a total of 1244 $Å^2$. Excluding residues 266–330, the r.m.s.d. for 302 C^{α} atoms is 0.50 Å between the Fab complex and the surface-mutant structure; thus, apart from this region the two structures are extremely similar. Although the local BACE2 structure around the Fab epitope differs considerably between the Fab complex and the uncomplexed structure, these differences do not propagate far into the active site. Relative to other structures, the 10s loop seems to be stabilized, as discussed below.

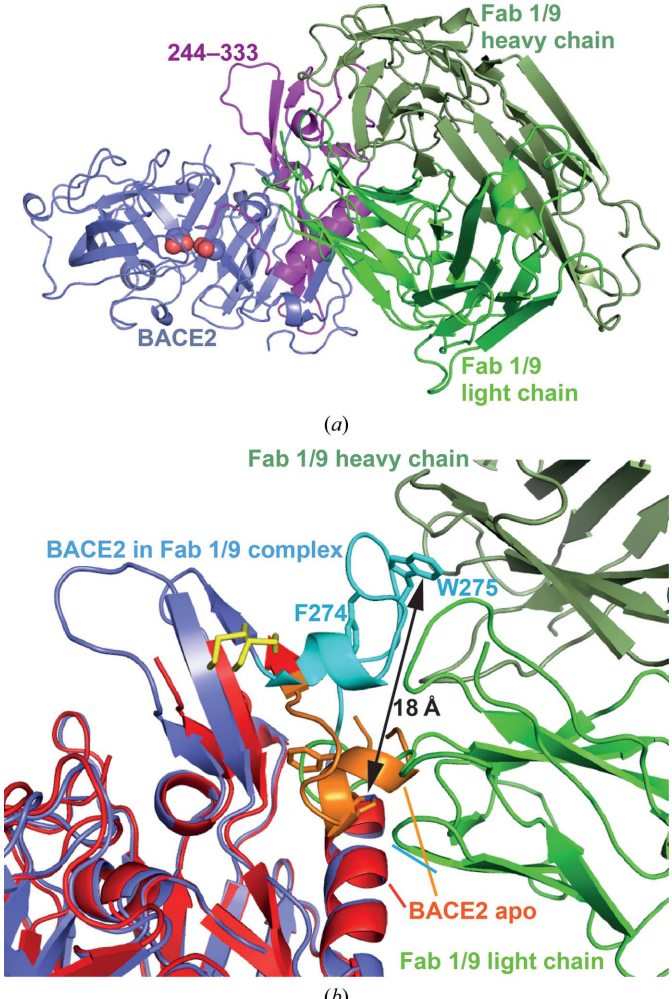

Figure 2
The BACE2–Fab 1/9 complex. (*a*) Overview. BACE2 is coloured slate blue with residues 244–333, the peptide used for immunization of mice, coloured magenta. The catalytic aspartates are shown as spheres. The Fab light chain is shown in light green and the heavy chain in dark green. (*b*) Superposition of the BACE2–Fab 1/9 complex (slate blue/cyan) with apo BACE2 E269A (red/gold). Residues 266–281 (apo, gold; Fab 1/9 complex, cyan) are highlighted to show the movement of the binding epitope upon Fab 1/9 binding. The short helix consists of residues 271–276 in the apo structure and residues 276–279 in the Fab 1/9 complex. The Cys282–Cys331 disulfide is shown in yellow and the Phe274 and Trp275 side chains are shown as these move by up to 18 Å.

3.4. Xaperone binary complexes

A total of 30 unique Xaperone clones from nine CDR3 sequence families showed confirmed target specificity in ELISA and retained binding to BACE2 in the presence of a small-molecule BACE2 inhibitor. Small-scale periplasmic expression and Ni–NTA chromatography purification of the Xaperones resulted in 0.5 ml 0.2–1 mg ml^{-1} Xaperone solutions that were used for off-rate screening by SPR, yielding off-rates ranging from 10^{-1} to 2×10^{-3} s^{-1}. In parallel, the Xaperones were tested by size-exclusion chromatography for their ability to form complexes with BACE2. Xaperones from different CDR3 sequence families building stable complexes and having good expression levels were selected for midscale protein expression and further characterization. The off-rate was not considered in the selection because dissociation was found to be a bi-exponential process in SPR. Typically, the final yield of isolated Xaperones was between 2 and 40 mg per litre of culture and their binding constants as determined by Biacore ranged from 1 to 116 n*M* (Supplementary Table S1).

BACE2 cross-competition experiments between Xaperones were performed by SPR with five Xaperones from different

families. Competition was observed between Xaperones XA4787, XA4781 and XA4793. None of the Xaperones in this group showed competition with XA4813 and XA4815. A lack of competition was also observed between Xaperones XA4813 and XA4815 (Supplementary Fig. S1). We conclude that three different epitopes are addressed by this set of five Xaperones. XA4787, XA4781 and XA4793 bind to the same epitope, whereas XA4813 and XA4815 bind to two additional different epitopes. Indeed, the ternary 1:1:1 complex BACE2–XA4813–XA4815 could be formed and analysed by SEC and AUC (Supplementary Figs. S1 and S2), and a crystal structure could be determined.

Only Xaperones XA4813 and XA4815 were selected for milligram-scale preparation and crystallization, as they formed stable complexes with BACE2. Crystals of the binary complex BACE2–XA4813 grew from a variety of conditions and were mounted directly from the screening drops for measurement. Five different crystal forms were fully characterized (Supplementary Table S7), all of which show quite similar BACE2–XA4813 interactions. Only the best diffracting is discussed here (Table 1; PDB entry 3zkq).

The BACE2–XA4813 binding interface (Fig. 3) is ∼780 Å^2 in size; it is rather flat, with no hydrophobic pocket and no salt bridge, but with many hydrogen bonds, and traps several water

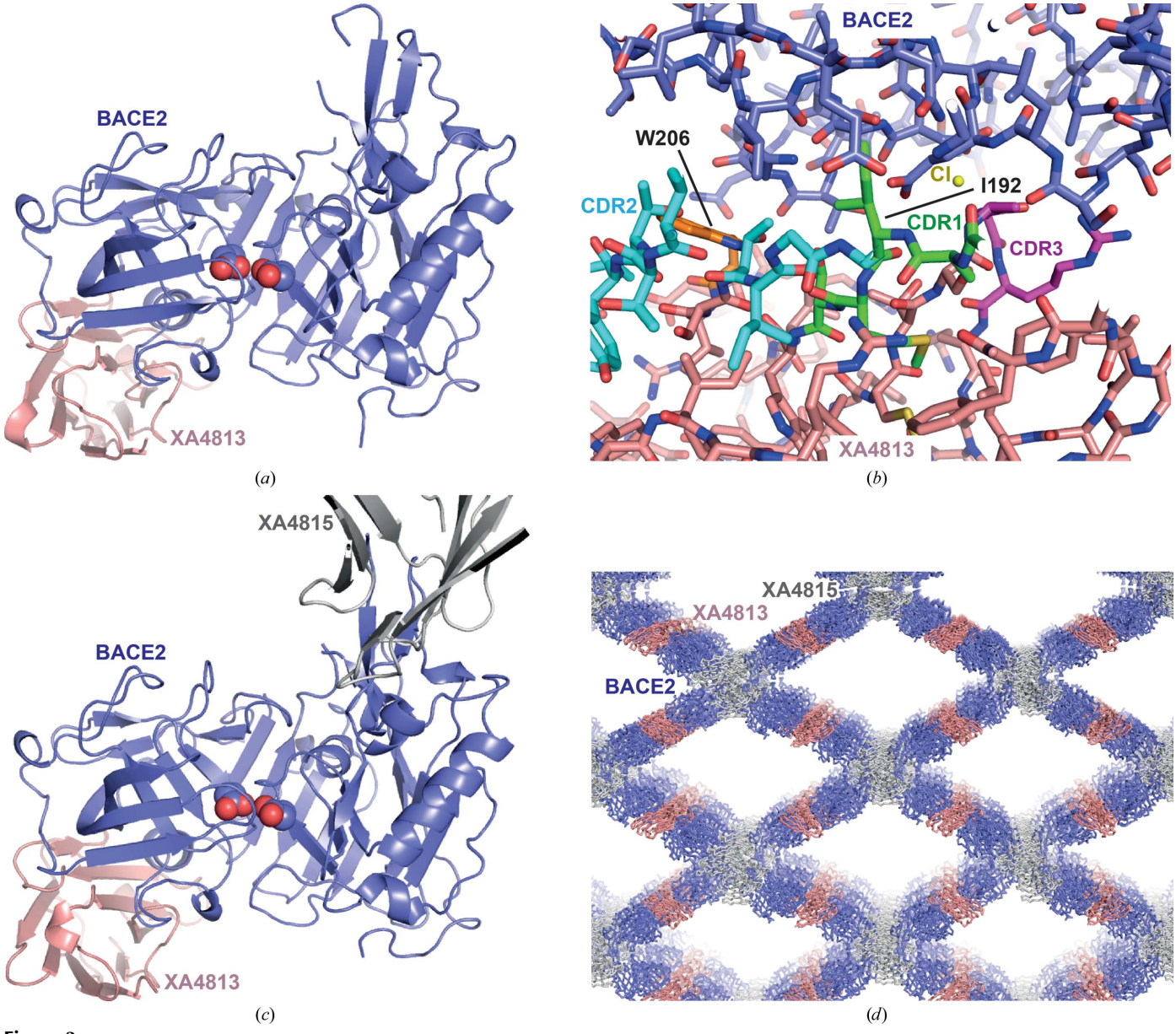

Figure 3
BACE2–Xaperone complex structures. (*a*) Overview of the binary BACE2–XA4813 complex. The BACE2 monomer is shown coloured slate blue, with the catalytic aspartate acids shown as spheres. The active site of BACE2 (slate blue) is 21 Å away from the binding interface of XA4813 (pink). (*b*) Stick representation of the binding interface, with CDR1, CDR2 and CDR3 of XA4813 shown in green, cyan and magenta, respectively. Ile192 of XA4813 binds to a surface pocket on BACE2. A Cl atom is shown as a yellow ball. (*c*) The ternary complex BACE2–XA4813–XA4815. (*d*) Packing of ternary complex crystals is dominated by Xaperone-mediated interactions. BACE2 is shown in slate blue, XA4813 in pink and XA4815 in grey.

molecules. The epitope is distant from the inhibitor-binding site, as expected, and is centred around BACE2 residues 112–114, which help to form a small pocket for Ile192 of XA4813, which is the central residue of CDR1 (SAIMT). CDR2 is long in this Xaperone, but only a few residues contact BACE2. CDR3 is short (AGR) but is involved in binding. Trp206 is in the interface, but is three residues before the start of CDR2. In some crystals a chlorine ion sits in the interface but does not appear to play a significant role, as it is replaced by water or bromine in other structures.

3.5. A Xaperone ternary complex

Crystals of the ternary complex BACE2 E269A–XA4813–XA4815 grew in space group *I*222 with one complex in the asymmetric unit. The BACE2–XA4813 interactions are essentially identical to those observed in the binary-complex structure (Figs. 3*a* and 3*c*). The epitope of XA4815 on BACE2 is located opposite to the XA4813 epitope, in which residues 186–189 of XA4815 (FTFS, before CDR1) interact antiparallel to BACE2 β-strand 279–282 (see also Phe270, Phe 274, Ala281 and Trp283). The resulting crystal packing is dominated by Xaperone-mediated interactions, illustrating the suitability of these binders as crystallization chaperones (Fig. 3*d*).

3.6. A Fynomer complex

Fynomers inhibiting BACE2 were isolated using standard phage-display techniques. The K_d for BACE2 binding of nine inhibitory Fynomers ranged from 6 to 380 n*M* (Supplementary Table S2), and all of them were specific for BACE2; none of them interacted with the serine protease chymase that was used as a control. As expected from their sequence similarity, the binding competition observed in SPR experiments indicated that all of the Fynomers have identical or at least overlapping binding sites on BACE2 (data not shown). Interestingly, Fynomers are sufficiently small to penetrate enzyme active sites, and for all Fynomers the BACE2 activity assay resulted in ideal inhibitor dose-response curves yielding reliable IC_{50} values (Supplementary Table S2).

Because all of the Fynomers had similar sequences and were competitive with each other in BACE2 binding, only three were chosen for crystallization trials. For the Fynomers 2B-D2, 2B-E9 and 2B-H11 that had high affinity and were monodisperse in AUC (data not shown), crystallization was performed in sitting-drop vapour-diffusion setups at 293 K at a protein concentration of 15–22 mg ml^{-1}. Tetragonal bipyramidal crystals were obtained from various screening conditions for the BACE2–Fynomer 2B-H11 complex, yielding diffraction patterns with ice rings, poor spot shape and anisotropy. The best crystals were produced by mixing 0.175 µl protein complex with 0.175 µl 1.8 *M* sodium/potassium phosphate pH 5.0. After two weeks no crystals were observed and the crystallization plates were shelved. Inspection after four months revealed crystals of dimensions 100 × 200 × 300 µm. The best diffraction was to 2.76 Å resolution (Table 1), but the data were corrupted by rings from scattering from beam apertures and also from a diffuse ring at 3.63 Å; although data to 2.76 Å were initially used in refinement, the final resolution was cut to 3.2 Å. While this is adequate to trace the Fynomer backbone, side-chain conformations are not always reliable.

We observe (Fig. 4) that Fynomer 2B-H11 binds in the BACE2 substrate channel on the nonprime side, with Arg42 of the Src loop extending from S4 towards S3 (as defined by Hong *et al.*, 2000). The Fynomer will thus partially compete with the substrate used in the enzyme assay, explaining the lack of correlation between K_d and IC_{50} of the Fynomers (Supplementary Table S2). The isolated Fynomers therefore represent promising candidates for specific and highly

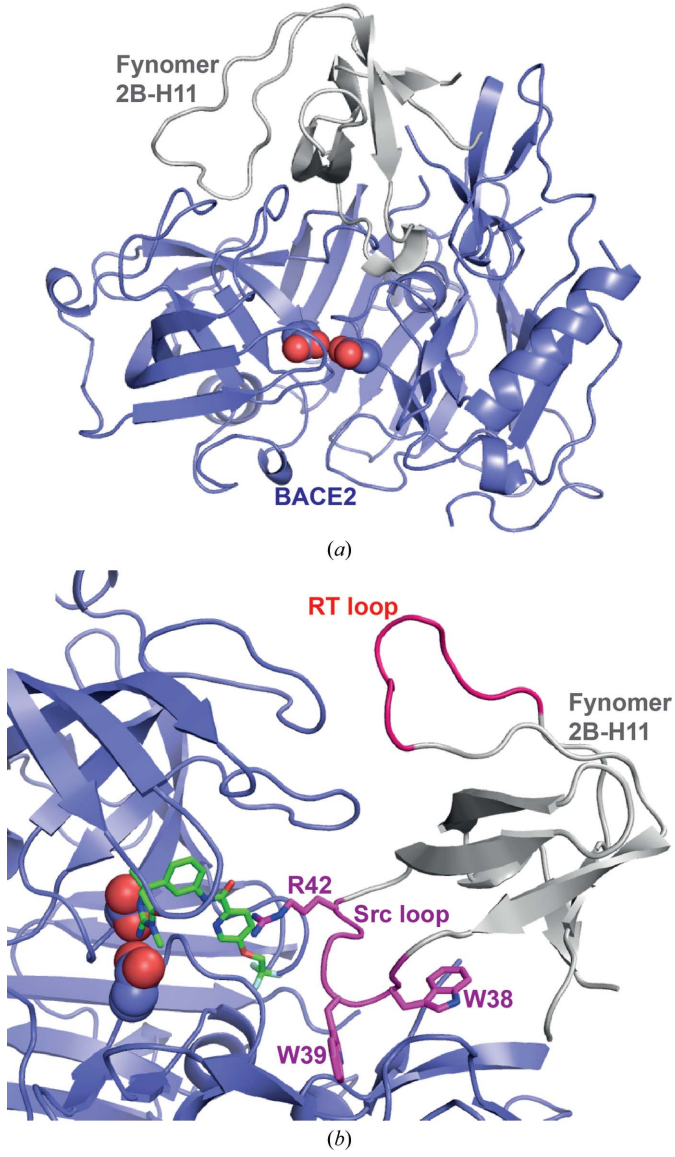

Figure 4
The BACE2–Fynomer 2B-H11 complex. (*a*) Overview. The Fynomer (grey) binds to the nonprime side of the BACE2 substrate-binding channel. (*b*) BACE2 is shown in slate blue, with the catalytic aspartate acids shown as spheres. The inhibitor RO5464694 (green) is superimposed from the E269A complex and it can be seen that this would clash with Arg42 in the Fynomer 2B-H11 Src loop (magenta). Trp38 and Trp39 of the Src loop are also shown as they make a major contribution to binding.

Table 2
Overview of BACE2 crystallization helpers.

	Fab 1/9	Xaperone XA4813	Fynomer 2B-H11	Surface mutant
Binder scaffold	IGg Fab	Single IG domain	SH3	
Binder scaffold size (kDa)	∼50	14	8	N/A
Binder variable region	6 loops (CDR)	3 loops (CDR)	2 loops (RT, Src)	N/A
Binder raising	Mouse hybridoma	Llama and phage display	DNA library and phage display	N/A
Binder expression	Cell line	*E. coli*	*E. coli*	*E. coli*
Expression level (mg ml^{-1})	>10	2–40	3.2	N/A
Immunogen	Peptide	BACE2/inhibited BACE2	BACE2	N/A
Selection bait	BACE2	BACE2/inhibited BACE2	BACE2	N/A
No. of selected binders (No. of sequence families)	3 (N/D)	30 (9)	9 (1)	N/A
K_d (nM)	N/D	1.2	6	N/A
k_{off} (s^{-1})	N/D	3.7×10^{-3}	2.8×10^{-3}	
k_{on} (M^{-1} s^{-1})	N/D	3.1×10^{6}	N/D	
Inhibition	No	No	IC_{50} = 174 nM	N/A
Time to crystal structure (months)	6–8	7	10	3
Structure resolution (Å)	1.8	1.5	3.2	1.9
Inhibitor cocrystallization	Soaking	Soaking	None	Soaking

selective BACE2 inhibition. In principle, it is straightforward to mutate a Fynomer sequence to improve binding (for example, for use as a tool inhibitor compound or as drug) or to improve crystal contacts, but this was not attempted here. The side chain of Arg42 of Fynomer 2B-H11 sits over the S3 pocket of BACE2 and is ∼9.5 Å from the catalytic aspartic acids (Fig. 4*b*). This might interfere with the binding of larger ligands; this could be avoided by mutation to a smaller residue. Soaking studies with small-molecule inhibitors were inconclusive owing to the poor diffraction quality of the crystals obtained.

4. Discussion

4.1. Protein binders and surface mutagenesis as crystallization helpers

This study demonstrates that in a case in which variation of protein-construct length by N- and C-terminal truncation alone did not yield crystals of sufficient quality (Ostermann *et al.*, 2006), high-resolution structures could be obtained after alterations of the protein surface either by complex formation with a binding protein or by mutation of surface residues. Having applied four different techniques to the crystallization target BACE2, we can now analyze the results in order to learn which method may be the most appropriate and how best to apply it in future crystallization challenges. In the case of BACE2 not only the mutagenesis of surface residues but also complex formation with surface-binding proteins leads to crystals that diffract to high resolution. Within three months of the start of surface-mutagenesis planning the mutant E269A yielded high-resolution crystals, demonstrating the power of the surface-mutant approach in protein crystallization. For the generation of the MAB for Fab-fragment production, a mouse was immunized with a commercially available peptide well before recombinant BACE2 was available. Purified BACE2 protein was later used for antibody screening. From immunization, it took six months to obtain a stable BACE2–Fab complex and one more month to obtain crystals that diffracted to high resolution. The resulting BACE2–Fab complex structures show that we were fortunate with the peptide selected for immunization, as part of the corresponding BACE2 sequence was stabilized in a previously unobserved conformation by Fab binding, but this did not affect the remaining BACE2 structure. For Fynomer selection, purified BACE2 was used in ELISA screening and Fynomers with single-digit nanomolar affinities were obtained within less than five months. All Fynomers turned out to be inhibitory in the enzymatic assay and usable cocrystals were obtained within ten months of the initiation of Fynomer selection. In contrast to the recently described Fynomer–chymase complexes, for which high-resolution structures could be determined (Schlatter *et al.*, 2012), the Fynomer–BACE2 cocrystals did not yield high-resolution data and only a peripheral part of the inhibitor-binding pocket was blocked by the Fynomer. For Xaperone production, purified BACE2 protein was used for the immunization of the llamas and for the screening of the Xaperones. Crystals were obtained within seven months of immunization. Much care was taken to define immunization and screening conditions that would deliver Xaperones for crystallization that would allow the structure determination of BACE2–inhibitor complexes. Both active BACE2 and an inhibitor complex were used for immunization, and only Xaperones that bound both BACE2 and the BACE2–inhibitor complex were selected. The diversity of the detected Xaperones was high, with nine different sequence families. XA4813 yielded six different crystal forms diffracting up to 1.5 Å resolution for both wild-type and mutant BACE2 (Supplementary Table S7). The binding epitope is distant from the inhibitor-binding site and from that of Fab 1/9. Table 2 summarizes the times, BACE2 proteins and crystallization trials needed to obtain high-resolution structures for each method tried. Each crystallization helper recognizes a unique epitope on BACE2 (Fig. 5). Only XA4813 binds to the N-terminal lobe; Fynomer 2B-H11 binds to the substrate pocket, while the Fab1/9 and XA4815 bind to the C-terminal lobe and their epitopes partly overlap with each other and that of the Fynomer. The BACE2 C-terminal residues 278–283 may constitute a hot spot for binding, as three of the four binding protein epitopes overlap there and these residues also

generate crystal contacts in PDB entry 2ewy and in the BACE2 E269A crystals (Supplementary Fig. S3).

In this example, cocrystals with protein binders often diffract to much better resolution than wild-type BACE2 alone. One explanation might be that the crystallization helpers restrict the motion of BACE2 in the crystal. Another is that the helpers provide different and better crystal lattice contacts. Both appear to contribute here. The related BACE1 (52% sequence identity) has been observed to adopt multiple conformational states in several regions in different crystal structures (Patel *et al.*, 2004; Xu *et al.*, 2012). From its biochemical properties, an even higher conformational flexibility has been postulated for BACE2 than for BACE1, especially for the C-terminal lobe (Ostermann *et al.*, 2006). We have performed an analysis of the *B* factors of BACE2 complex structures, which shows that each of the binders restricts the mobility of the BACE2 region to which it binds (Supplementary Fig. S4). This observed local decrease in BACE2 mobility, especially in the more mobile C-terminal BACE2 regions, could explain why the Fab and Xaperone complexes of wild-type BACE2 diffract to much better resolution than wild-type BACE2 alone. Fynomer 2B-H11 makes no contribution to stabilizing the more mobile C-terminal BACE2 regions (Supplementary Fig. S4) and does not yield well diffracting crystals.

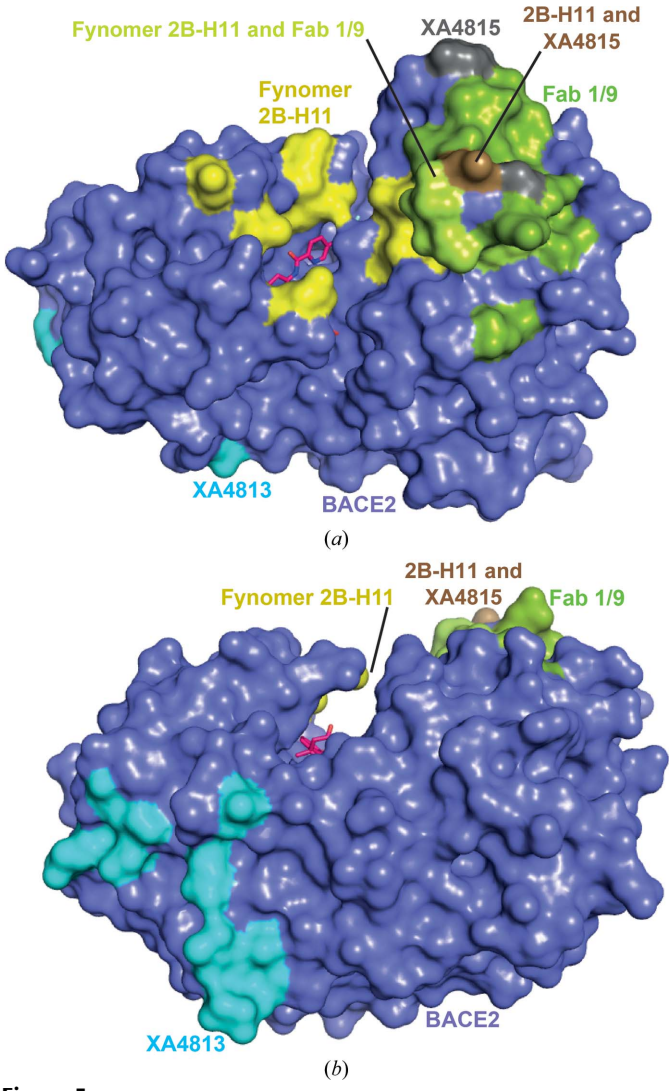

Figure 5
The binding epitopes of the crystallization helpers Fab 1/9 (green), XA4813 only (cyan), XA4815 only (grey) and Fynomer 2B-H11 only (yellow) mapped onto the BACE2 E269A–RO5464694 complex surface (slate blue). The inhibitor is shown as red sticks. BACE2 residues 275–278 that interact with both the Fynomer and Fab 1/9 only are coloured lime. Residue 279 that interacts with both Fynomer 2B-H11 and XA4815 only is coloured brown. Residues 268–269 are in the Fab 1/9 binding epitope but are not in the structure used to generate the surface. Interacting residues are defined with a 3.5 Å cutoff between any pair of atoms. (*a*) Orientation as in Fig. 1. (*b*) Rotated by 90°. The centre of the XA4813 epitope has bridging waters and sometimes contains a chlorine ion.

It is possible that binding-protein affinity might correlate with crystallization success, but in this example success did not correlate at all with either the thermodynamic K_d or the kinetic k_{off}. However, we did observe that only protein complexes that can be purified intact by size-exclusion chromatography gave crystals (corresponding to a K_d of ∼20–50 n*M*). In several instances crystallization trials with the ternary BACE2–XA4813–XA4815 complex only gave crystals of the binary BACE2–XA4813 complex, and in one instance (data not shown) the asymmetric unit contained four instances of the BACE2–XA4813 complex, only two of which had partial density for XA4815 (the K_d values are 1.2 n*M* for XA4813 and 26 n*M* for XA4815). Xaperone XA4813 and Fab 1/9 bind to different epitopes on BACE2 and both yield high-resolution crystals. Although Fynomer 2B-H11 did not yield high-resolution crystals, the isolation of Fynomers binding to alternative epitopes on BACE2 may allow the preparation of crystals suitable for high-resolution ligand-binding studies. It was possible to obtain a useful crystallization helper Fab from a monoclonal antibody previously generated for other purposes and fortunate that this first Fab investigated bound to BACE2 without interfering with inhibitor binding and gave usable crystals, although they were often twinned and were only obtained under only one specific set of conditions. With Xaperones, where much care was taken to use correctly folded BACE2 in the llama immunization and to screen for a diverse set of Xaperones that bind inhibited BACE2, crystals with different crystal forms were readily obtained under a variety of conditions. We find Xaperones to be monodisperse and monomeric in AUC (data not shown) and importantly no Xaperone-only crystals were found, whereas cocrystallization with Fab yielded Fab-only crystals under several conditions. As regards any correlation between the size and geometry of the binders and success in crystallization, we find here that (i) while Fabs provide the most additional surface area to form crystal lattice contacts, and will have diverse binding epitopes, only one specific set of conditions led to crystals; (ii) while Fynomers are more compact and may be able to bind regions not accessible to the other scaffolds, here this led to binding in the substrate cleft and no stabilization of mobile BACE2 regions; and (iii) since Xaperones provide more bulk to form crystal lattice contacts than do Fynomers and are simultaneously more rigid than Fab fragments, which may display variations in the elbow angle, and since they bind to diverse

epitopes and easily give a range of different crystal forms, they appear to be the best compromise between bulk and flexibility.

Although high-resolution structures of drug targets in complex with inhibitory protein binders have been reported (Bandeiras *et al.*, 2008; Schlatter *et al.*, 2012), despite the fact that inhibition was not specifically a selection criterion, our results indicate that it may be better to produce binding proteins that are tailored towards the desired application. If protein binders themselves are generated primarily as tool inhibitor compounds, the IC_{50} should be considered as a selection criterion in addition to the affinity. On the other hand, when generating crystallization helpers either a high diversity of binders or noncompetitiveness with biological ligands or inhibitors could be considered from the start, as both may enhance the chance of obtaining well resolved cocrystal structures.

4.2. New insights gained from the high-resolution BACE2 structures

As in all aspartic proteases, a flexible β-hairpin loop (flap) comprising residues Val83–Gly94 covers the active site of BACE2. For BACE1 a range of flap conformations from fully closed with large peptidomimetic inhibitors to fully open in the unliganded protease have been reported (Hong *et al.*, 2000; Patel *et al.*, 2004). Because the rigid Pro70 in the BACE1 flap is replaced by Lys86 in BACE2, the flap was expected to be even more flexible in BACE2. Surprisingly, we have not trapped a fully open flap or a fully disordered flap in any of our crystals, but partial disorder is the norm, particularly in the absence of ligand. While Ostermann *et al.* (2006) reported the BACE2 flap only in the half-closed conformation typical of the complex with a low-molecular-weight BACE inhibitor, we observe a considerable range of flap conformations in our structures (Fig. 6). None of the binding proteins in our crystals contacts the flap, so we did not expect them to affect the flap conformation. However, it turned out that different crystallization helpers favoured different flap geometries: the most open flaps were observed in the inhibited and uninhibited Fab complexes. Surprisingly, the most closed conformation was observed in the uninhibited ternary BACE2–XA4813–XA4815 complex. This superimposes well with the fully closed BACE1 flap conformation observed with the large peptidic inhibitor in PDB entry 1fkn. The limited range of flap movement observed, especially the lack of any open flap conformation in four different crystals of uninhibited BACE2, tends to indicate that the substitution of the flap proline by a lysine does not increase the flap mobility in BACE2, but rather that both BACE isoforms have a more rigid flap than other aspartic proteases (Patel *et al.*, 2004).

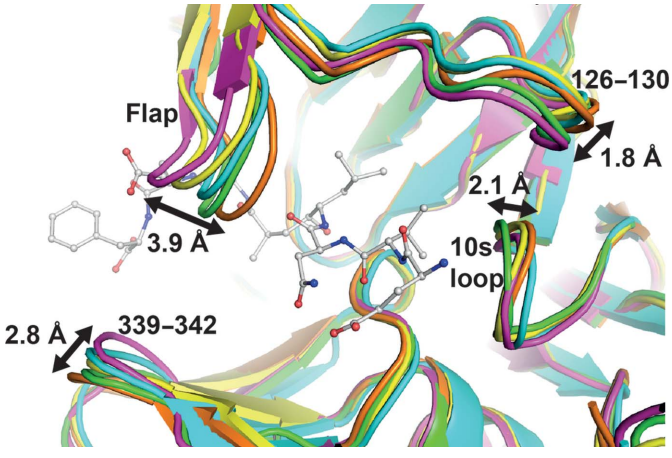

Figure 6
Conformational flexibility around the BACE2 active site captured by crystal structures from different crystal forms. Movements of the flap, the 10s loop, loop 126–130 and loop 339–342 are apparent. Magenta, PDB entry 3zkq; yellow, PDB entry 3zkg; cyan, PDB entry 3zl7; green, PDB entry 3zkm; orange, PDB entry 3zkx. For orientation, the BACE1 peptidic inhibitor OM99-2 (PDB entry 1fkn) is superimposed in grey.

The main inhibitor-binding pocket in BACE1 and BACE2 is the combined S1/S3 pocket, and the hydrophobic residues (Leu46, Tyr87, Phe124, Trp131 and Ile134) lining this pocket are identical in both BACE isoforms. High-resolution structures confirm identical side-chain conformations for these residues in BACE2 and BACE1. This pocket is close to both the loop Phe124–Trp131 and to the 10s loop (Gly24–Gly29). These less conserved and more flexible loops at the periphery of the inhibitor site are therefore of great interest for the design of selective BACE1 or BACE2 inhibitors. The 10s loop can be both 'up' (open) and 'down' (closed) in BACE1 and was only observed in the 'down' conformation in the initial low-resolution BACE2 structure (Patel *et al.*, 2004; Ostermann *et al.*, 2006). For the 10s loop we observe mostly the '10s loop down' conformation as in BACE1 (PDB entry 1fkn). However, different inhibitors induce an ensemble of conformations where this loop is moved out by about 1 Å in response to inhibitor binding, more as observed in BACE2 (PDB entry 2ewy). In many of the Xaperone complexes the 10s loop is very poorly ordered, and in one case (data not shown) the amino acids from the N-terminus up to and including the 10s loop are flipped out and partially observed in a nearby crystal contact. In the Fynomer complex, the N-terminal residues, although not directly contacting the Fynomer, adopt a β-structure different from that otherwise observed. We conclude that the 10s loop in BACE2, together with the preceding residues, does not form a particularly stable structure.

We observe conformations of loop 124–131 in many different BACE2 crystals with different packing environments that are all similar to each other but distinct from the BACE1 conformation in PDB entry 1fkn. This conformational difference between BACE2 and BACE1 is the closest to the active site and offers an opportunity to design BACE2/BACE1 selectivity into low-molecular-weight inhibitors. Our ensemble of structures shows that the differences in the conformation of loop 124–131 between BACE1 and BACE2 are not caused by the packing interactions in PDB entry 2ewy (Fig. 6) and thus may be used in the design of selective BACE inhibitors.

The fact that the loops normally involved in ligand binding are quite mobile in a variety of crystals suggests that this may be the normal case in solution, which would at least provide easy access for substrates: all of the crystal forms documented

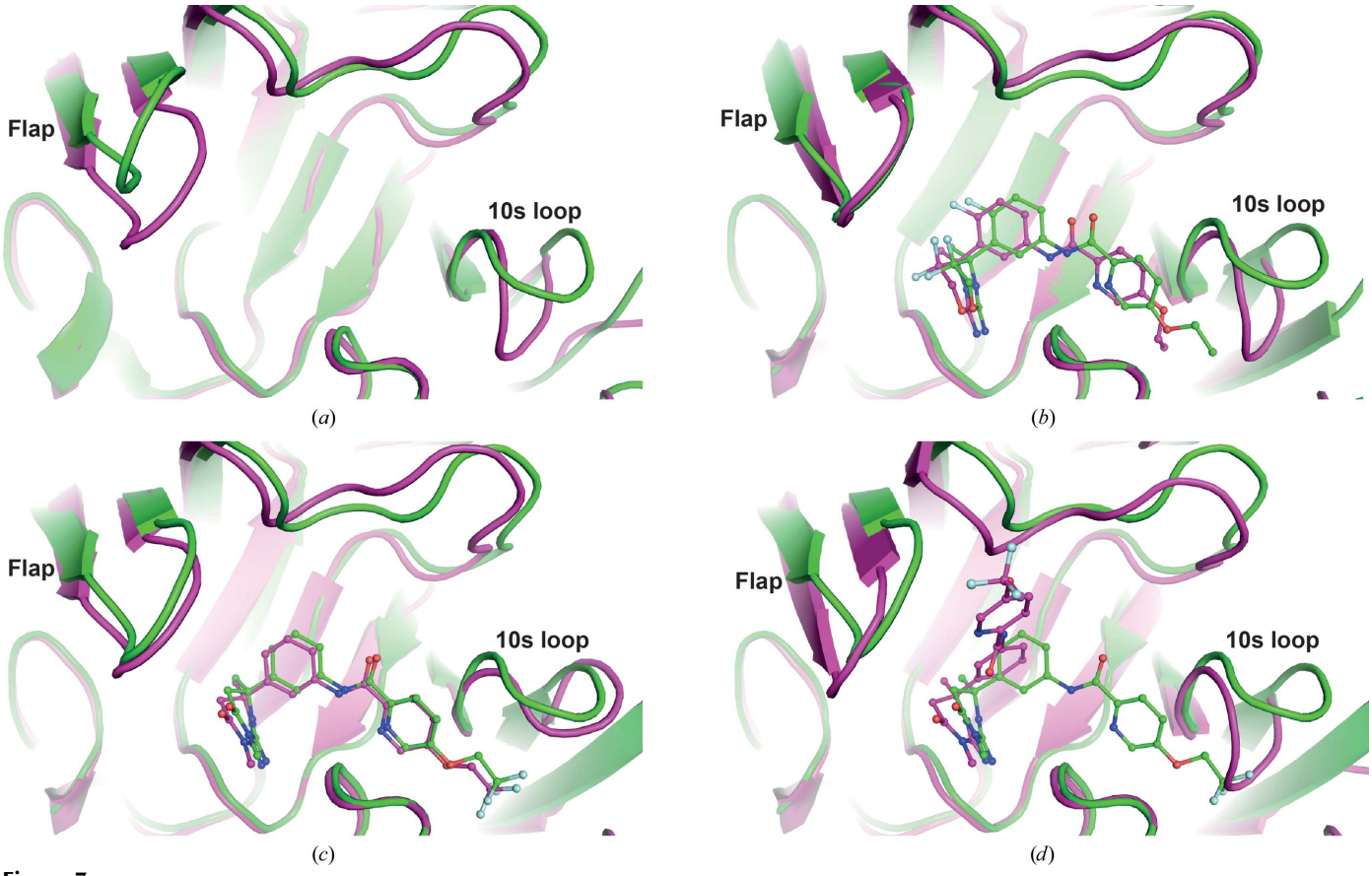

Figure 7
Superposition of BACE2 (magenta) and BACE1 (green) crystal structures. (*a*) Apo structures: PDB entries 3zkg and 1w50. (*b*) Ethoxypyridine-substituted inhibitor complexes: PDB entries 3zlq and 4j0t. (*c*) Trifluoroethoxypyridine-substituted inhibitor complexes: PDB entries 3zki and 3zov. (*d*) Trifluoroethoxypyridine-substituted inhibitor complexes: PDB entries 3zkn and 3zov.

here appear to be suitable for ligand-soaking studies and this has been demonstrated in four cases.

4.3. Independent crystal forms benefit structure-based inhibitor design

Having more than one crystal form had several benefits for structure-based BACE-inhibitor design. Firstly, a series of independent high-resolution crystal structures gave a more detailed description of the conformational flexibility of BACE2. Secondly, cocrystal structures of more inhibitors could be solved, for example when inhibitors with low solubility needed a specific pH or a high DMSO concentration to enter the crystal. Thirdly, structures can be solved even when inhibitors need one specific protein conformation that is not present in one crystal form but is in others. Fourthly, one BACE2 inhibitor displayed different binding geometry in different crystal forms, which can be understood as follows. The 10s loop in the five crystal structures of uninhibited BACE2 described here is always in the 'down' position, despite some degree of variation (Fig. 7). In the BACE1 apo structure with PDB code 1w50 (Patel *et al.*, 2004), however, the 10s loop was observed in the 'up' position (Fig. 7*a*). Hilpert *et al.* (2013) have shown that BACE1 inhibitors can be made to be selective against BACE2 by pushing against the 10s loop in BACE2. The ethoxypyridine substituent of a BACE1 inhibitor fits nicely into the BACE1 10s loop in its 'up' position, but binds in a less favourable conformation to the BACE2 10s loop in its slightly shifted 'down' position (Fig. 7*b*). This results in fivefold selectivity of BACE1 over BACE2 (Hilpert *et al.*, 2013). Here, we show that a larger trifluoroethoxypyridine-substituted BACE1 inhibitor (IC_{50} = 0.06 μM) induces a BACE1-like 'up' position of the BACE2 10s loop (Fig. 7*c*), but this comes with a high binding-energy penalty for BACE2 (IC_{50} = 1.2 μM). However, when bound to the Fab-complexed BACE2 the same trifluoroethoxypyridine-substituted inhibitor does not enter the S3 pocket, the 10s loop remains in the 'down' position and the ligand instead adopts an unusual binding mode in which the trifluoroethoxypyridine side chain interacts with the flap region (Fig. 7*d*). Complex formation between BACE2 and the Fab must significantly restrict the conformational space available to the 10s loop, implying that for ligands with extended S3 substituents one or more of the other available crystal systems should be used, as in these the 10s loop is not compromised.

5. Conclusions

Typically, structural flexibility in the flap region of aspartyl proteinases is observed by determining the crystal structure of

the apo form and of complexes with ligands that stabilize different flap conformations. However, this requires a diverse set of ligands, which is often only available for well studied drug targets. Here, we show that in the absence of such ligands conformational flexibility can also be visualized by determining crystal structures in different crystal forms induced by surface mutagenesis or crystallization helpers. This provides information about protein dynamics (Fig. 6, Supplementary Fig. S4) and, more importantly for structure-based drug design, documents the conformational space available to the target. The strategy applied in this work is applicable not only to aspartyl proteinases but to flexible proteins in general.

We thank Jeremy Beauchamp for the BACE2 DNA construct and many discussions. We thank Marco Crisci and Andrea Wiget for SPR measurements and the staff at Expose for X-ray data collection. The data were collected on beamline X10SA at the Swiss Light Source.

References

Abdul-Hay, S. O., Sahara, T., McBride, M., Kang, D. & Leissring, M. A. (2012). *Mol. Neurodegener.* **7**, 46.

Akpinar, P., Kuwajima, S., Krützfeldt, J. & Stoffel, M. (2005). *Cell Metab.* **2**, 385–397.

Bandeiras, T. M. *et al.* (2008). *Acta Cryst.* D**64**, 339–353.

Baranova, E., Fronzes, R., Garcia-Pino, A., Van Gerven, N., Papapostolou, D., Péhau-Arnaudet, G., Pardon, E., Steyaert, J., Howorka, S. & Remaut, H. (2012). *Nature (London)* **487**, 119–122.

Broger, C. (2011). *XSAE* v.1.6.2. F. Hoffmann-La Roche AG, Basel, Switzerland.

Danley, D. E. (2006). *Acta Cryst.* D**62**, 569–575.

Derewenda, Z. S. (2004). *Structure*, **12**, 529–535.

Domanska, K., Vanderhaegen, S., Srinivasan, V., Pardon, E., Dupeux, F., Marquez, J. K., Giorgetti, S., Stoppini, M., Wyns, L., Bellotti, V. & Steyaert, J. (2011). *Proc. Natl Acad. Sci. USA*, **108**, 1314–1319.

Emsley, P. & Cowtan, K. (2004). *Acta Cryst.* D**60**, 2126–2132.

Esterházy, D. *et al.* (2011). *Cell Metab.* **14**, 365–377.

Fukui, K. *et al.* (2005). *Cell Metab.* **2**, 373–384.

Gebauer, M. & Skerra, A. (2012). *Methods Enzymol.* **503**, 157–188.

Gilbreth, R. N. & Koide, S. (2012). *Curr. Opin. Struct. Biol.* **22**, 413–420.

Goldschmidt, L., Cooper, D. R., Derewenda, Z. S. & Eisenberg, D. (2007). *Protein Sci.* **16**, 1569–1576.

Grabulovski, D., Kaspar, M. & Neri, D. (2007). *J. Biol. Chem.* **282**, 3196–3204.

Hamers-Casterman, C., Atarhouch, T., Muyldermans, S., Robinson, G., Hamers, C., Songa, E. B., Bendahman, N. & Hamers, R. (1993). *Nature (London)*, **363**, 446–448.

Hassell, A. M. *et al.* (2007). *Acta Cryst.* D**63**, 72–79.

Hausammann, G. J., Heitkamp, T., Matile, H., Gsell, B., Thoma, R., Schmid, G., Frasson, D., Sievers, M., Hennig, M. & Grütter, M. G. (2013). *Biochem. Biophys. Res. Commun.* **431**, 70–75

Hilpert, H. *et al.* (2013). Submitted.

Hinz, A., Lutje Hulsik, D., Forsman, A., Koh, W. W.-L., Belrhali, H., Gorlani, A., De Haard, H., Weiss, R. A., Verrips, T. & Weissenhorn, W. (2010). *PLoS One*, **5**, e10482.

Hong, L., Koelsch, G., Lin, X., Wu, S., Terzyan, S., Ghosh, A. K., Zhang, X. C. & Tang, J. (2000). *Science*, **290**, 150–153.

Hunte, C. & Michel, H. (2002). *Curr. Opin. Struct. Biol.* **12**, 503–508.

Kabsch, W. (2010). *Acta Cryst.* D**66**, 125–132.

Koide, A., Gilbreth, R. N., Esaki, K., Tereshko, V. & Koide, S. (2007). *Proc. Natl Acad. Sci. USA*, **104**, 6632–6637.

Korotkov, K. V., Pardon, E., Steyaert, J. & Hol, W. G. J. (2009). *Structure*, **17**, 255–265.

Kovari, L. C., Momany, C. & Rossmann, M. G. (1995). *Structure*, **3**, 1291–1293.

Kuglstatter, A., Stahl, M., Peters, J.-U., Huber, W., Stihlem, M., Schlatter, D., Benz, J., Ruf, A., Roth, D., Enderle, T. & Hennig, M. (2008). *Bioorg. Med. Chem. Lett.* **18**, 1304–1307.

Lam, A. Y., Pardon, E., Korotkov, K. V., Hol, W. G. J. & Steyaert, J. (2009). *J. Struct. Biol.* **166**, 8–15.

Loris, R., Marianovsky, I., Lah, J., Laeremans, T., Engelberg-Kulka, H., Glaser, G., Muyldermans, S. & Wyns, L. (2003). *J. Biol. Chem.* **278**, 28252–28257.

McCoy, A. J., Grosse-Kunstleve, R. W., Adams, P. D., Winn, M. D., Storoni, L. C. & Read, R. J. (2007). *J. Appl. Cryst.* **40**, 658–674.

Meher, A. K., Blaber, S. I., Lee, J., Honjo, E., Kuroki, R. & Blaber, M. (2009). *Acta Cryst.* F**65**, 1136–1140.

Mittl, P. R. E., Berry, A., Scrutton, N. S., Perham, R. N. & Schulz, G. E. (1994). *Acta Cryst.* D**50**, 228–231.

Murshudov, G. N., Skubák, P., Lebedev, A. A., Pannu, N. S., Steiner, R. A., Nicholls, R. A., Winn, M. D., Long, F. & Vagin, A. A. (2011). *Acta Cryst.* D**67**, 355–367.

Musacchio, A., Saraste, M. & Wilmanns, M. (1994). *Nature Struct. Biol.* **1**, 546–551.

Muyldermans, S. (2001). *J. Biotechnol.* **74**, 277–302.

Nygren, P. A. (2008). *FEBS J.* **275**, 2668–2676.

Ostermann, N., Eder, J., Eidhoff, U., Zink, F., Hassiepen, U., Worpenberg, S., Maibaum, J., Simic, O., Hommel, U. & Gerhartz, B. (2006). *J. Mol. Biol.* **355**, 249–261.

Patel, S., Vuillard, L., Cleasby, A., Murray, C. W. & Yon, J. (2004). *J. Mol. Biol.* **343**, 407–416.

Perspicace, S., Banner, D., Benz, J., Müller, F., Schlatter, D. & Huber, W. (2009). *J. Biomol. Screen.* **14**, 337–349.

Rasmussen, S. G. F., Choi, H.-J. *et al.* (2011). *Nature (London)*, **469**, 175–180.

Rasmussen, S. G. F., DeVree, B. T. *et al.* (2011). *Nature (London)*, **477**, 549–555.

Schlatter, D., Brack, S., Banner, D. W., Batey, S., Benz, J., Bertschinger, J., Huber, W., Joseph, C., Rufer, A., van der Klooster, A., Weber, M., Grabulovski, D. & Hennig, M. (2012). *MAbs*, **4**, 497–508.

Schlatter, D., Thoma, R., Küng, E., Stihle, M., Müller, F., Borroni, E., Cesura, A. & Hennig, M. (2005). *Acta Cryst.* D**61**, 513–519.

Sennhauser, G. & Grütter, M. G. (2008). *Structure*, **16**, 1443–1453.

Smart, O. S., Womack, T. O., Flensburg, C., Keller, P., Paciorek, W., Sharff, A., Vonrhein, C. & Bricogne, G. (2012). *Acta Cryst.* D**68**, 368–380.

Spinelli, S., Desmyter, A., Verrips, C. T., de Haard, H. J., Moineau, S. & Cambillau, C. (2006). *Nature Struct. Mol. Biol.* **13**, 85–89.

Steyaert, J. & Kobilka, B. K. (2011). *Curr. Opin. Struct. Biol.* **21**, 567–572.

Tereshko, V., Uysal, S., Koide, A., Margalef, K., Koide, S. & Kossiakoff, A. A. (2008). *Protein Sci.* **17**, 1175–1187.

Wiesmann, C., Beste, G., Hengstenberg, W. & Schulz, G. E. (1995). *Structure*, **3**, 961–968.

Winn, M. D. *et al.* (2011). *Acta Cryst.* D**67**, 235–242.

Xu, Y., Li, M., Greenblatt, H., Chen, W., Paz, A., Dym, O., Peleg, Y., Chen, T., Shen, X., He, J., Jiang, H., Silman, I. & Sussman, J. L. (2012). *Acta Cryst.* D**68**, 13–25.

Zhu, X., Dickerson, T. J., Rogers, C. J., Kaufmann, G. F., Mee, J. M., McKenzie, K. M., Janda, K. D. & Wilson, I. A. (2006). *Structure*, **14**, 205–216.